AD-A042 809 TRW DEFENSE AND SPACE SYSTEMS GROUP REDONDO BEACH CALIF F/G 20/9
PULSED PLASMA LOSS AND ACCELERATION MECHANISMS IN STRONG BIAS M--ETC(U)
JUL 77 C L DAILEY, R H LOVBERG F44620-76-C-0107
UNCLASSIFIED AFOSR-TR-77-0828 NL

| OF |
AD
A042809

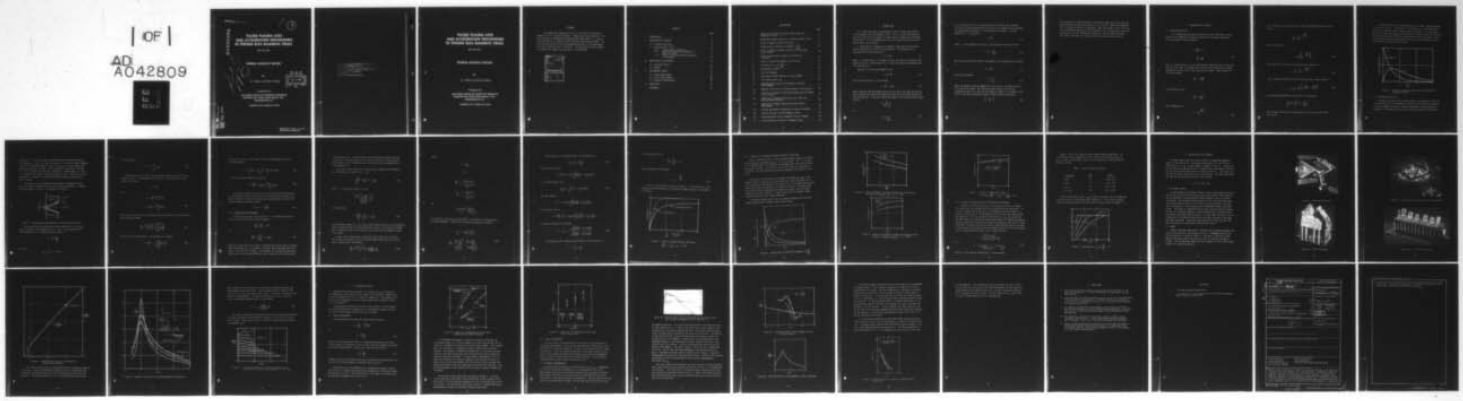

END
DATE
FILMED
9 -77
DDC

(4)

PULSED PLASMA LOSS AND ACCELERATION MECHANISMS IN STRONG BIAS MAGNETIC FIELDS

JULY 29, 1977

INTERIM SCIENTIFIC REPORT

By:

C.L. Dailey and R.H. Lovberg

Prepared for

AIR FORCE OFFICE OF SCIENTIFIC RESEARCH
BOLLING AIR FORCE BASE (BLDG. 410)
WASHINGTON D.C.

CONTRACT NO. F44620-76-C-0107

AIR FORCE OFFICE OF SCIENTIFIC RESEARCH (AFSC)
NOTICE OF TRANSMITTAL TO DDC
This technical report has been reviewed and is approved for public release IAW AFR 190-12 (7b).
Distribution is unlimited.
A. D. BLOSE
Technical Information Officer

PULSED PLASMA LOSS AND ACCELERATION MECHANISMS IN STRONG BIAS MAGNETIC FIELDS

JULY 29, 1977

INTERIM SCIENTIFIC REPORT

By:

C.L. Dailey and R.H. Lovberg

Prepared for

AIR FORCE OFFICE OF SCIENTIFIC RESEARCH
BOLLING AIR FORCE BASE (BLDG. 410)
WASHINGTON D.C.

CONTRACT NO. F44620-76-C-0107

FOREWORD

This program was sponsored by the Air Force Office of Scientific Research; Dr. B.T. Wolfson and Major T. Meier were Program Monitors. The work was done at TRW Defense and Space Systems Group by Dr. C.L. Dailey with Professor R.H. Lovberg of UCSD providing consulting assistance. Design and construction of the test equipment and much of the experimental work was carried out by W.P. Goldstein. The assistance of Ethel Johnson in readying this report for publication is appreciated.

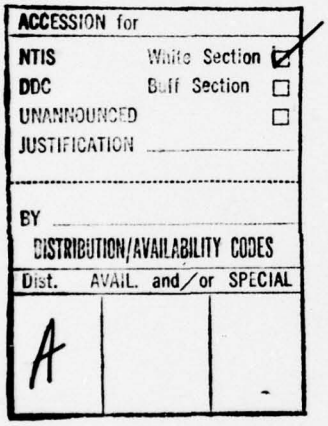

CONTENTS

ILLUSTRATIONS

1. INTRODUCTION

This report describes an experimental study of plasma acceleration in the presence of a bias magnetic field. This is a field that does not vary with time but has a spatial variation that is selected for efficient acceleration. It is superimposed on the self-fields that arise from the plasma and circuit currents.

A simple physical argument can be made to show that the efficiency cannot exceed 50% for self-field acceleration. At any point in an accelerator the current density is

$$j = \sigma(E - vB) \tag{1}$$

where σ is conductivity, v is plasma velocity and E and B are electric and magnetic fields. The directions of v, E and B are mutually orthogonal and j is parallel to E.

Equation (1) can be rearranged to give

$$E = \frac{j}{\sigma} + vB \tag{2}$$

After multiplication by j this becomes

$$jE = \frac{j^2}{\sigma} + (jB)v \tag{3}$$

which expresses the input power density as the sum of the ohmic dissipation power densiety and the rate of mechanical work per unit volume done by the jB force density. If the only losses were ohmic, the efficiency would therefore be

$$\eta = \frac{jB}{jBv + \frac{j^2}{\sigma}}$$

or

$$\eta = \frac{1}{1 + \frac{j}{\sigma Bv}} \tag{4}$$

For the simple case of a slab model with no bias field, with property variations in the acceleration direction only, the magnetic field gradient is approximately B/δ where δ is the interaction distance. Thus the Maxwell Curl - H relation is

$$j = \frac{1}{\mu}\frac{B}{\delta} \tag{5}$$

where μ is the permeability of space, and equation (4) can be written

$$\eta = \frac{1}{1 + \frac{1}{\mu\sigma\delta v}} \tag{6}$$

but since the diffusion speed of the magnetic field relative to the plasma is

$$v_d = \frac{1}{\mu\sigma\delta} \tag{7}$$

Equation (6) becomes

$$\eta = \frac{1}{1 + \frac{1}{R_N}} \tag{8}$$

Where the magnetic Reynolds number R_N is the ratio of the plasma velocity to the diffusion speed. By multiplying the velocity terms by the acceleration time it is seen that the Reynolds number is also equal to the ratio of the field penetration depth to the acceleration distance,

$$R_N = \frac{v}{v_d} = \frac{\Delta}{\delta} \tag{9}$$

For any practical plasma accelerator the magnetic body force jB is the only force producing acceleration and this ratio is unity. Hence, from Equation (8), the ohmic efficiency is 50 percent. When the magnetic field is the sum of the self-field and a bias field, Equation (5) is no longer valid and the possibility arises of removing the 50 percent limit on ohmic efficiency. This report describes the results achieved in that direction to date.

2. DESCRIPTION OF THRUSTER

2.1 CONSTANT BIAS FIELD

It is interesting that the application of a bias field that is both spatially and temporally constant does not alter the ohmic efficiency. At any location in the accelerator

$$\rho v \frac{dv}{dZ} = jB$$

or

$$\frac{dv}{dZ} = \frac{jB}{\dot{m}} \tag{10}$$

where ρ is mass density, Z is the acceleration direction and $\dot{m}$ is mass flow rate per unit area. For steady flow, and for a bias field that is large compared to the self-field, both $\dot{m}$ and B are constant. When Equation (1) is differentiated

$$\frac{dj}{dZ} = -\sigma B \frac{dv}{dZ}$$

or with Equation (10)

$$\frac{dj}{dZ} = -\frac{\sigma B^2}{\dot{m}} j$$

which integrates to

$$j = j_o e^{-\frac{\sigma B^2}{\dot{m}} Z} \tag{11}$$

This relation for the current density can be combined with Equation (10) to give

$$\frac{dv}{dZ} = \frac{j_0 B}{\dot{m}} e^{-\frac{\sigma B^2}{\dot{m}} Z}$$

which integrates to

$$v = \frac{j_0}{\sigma B}\left(1-e^{-\frac{\sigma B^2}{\dot{m}} Z}\right) \tag{12}$$

From Equation (11) the ohmic dissipation power density is

$$P = \frac{j^2}{\sigma} = \frac{j_0^2}{\sigma} e^{\frac{-2\sigma B^2}{\dot{m}} Z} \tag{13}$$

and by combining Equations (11) and (12) the kinetic power density is

$$P_k = jvB = \frac{j_0^2}{\sigma}\left(e^{\frac{-\sigma B^2 Z}{\dot{m}}} - e^{\frac{2\sigma B^2 Z}{\dot{m}}}\right) \tag{14}$$

By integrating Equations (13) and (14) it is found that

$$\int_0^\infty P_D dZ = \int_0^\infty P_k dZ = \frac{j_0^2}{2\sigma^2 B^2}$$

and the ohmic efficiency is 50 percent as it was for the self-field accelerator.

The variations with Z of the dissipative and kinetic power densities are shown in Figure 1. The former is a maximum at Z = 0 and drops one e-fold by the time the kinetic power reaches its maximum. It is seen that not only B, but σ and $\dot{m}$ have no effect on the 50 percent limit on efficiency. The e-fold distance is $\sigma B^2/\dot{m}$ and increasing the bias field with all other variables held constant simply reduces the scale of the acceleration distance without affecting the efficiency.

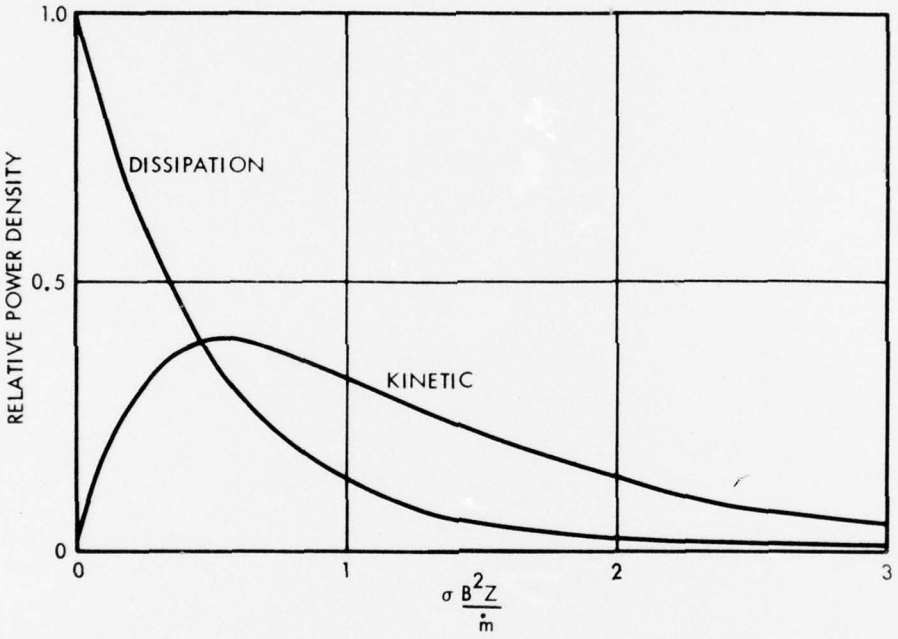

Figure 1. Relative Dissipation and Kinetic Power Densities (Constant E and B)

2.2 DECREASING BIAS FIELD

The ohmic efficiency limit of 50 percent is not inherent in the bias field concept but is a consequence of the bias field being held constant. It can be removed by using a field that decreases in the acceleration direction. The reason for this can be seen intuitively by referring to

Equation (1). The current density (and hence the acceleration) drops to zero whenever v = E/B, i.e., when the back emf (in electric motor language) is equal to the applied electric field. This velocity (the plasma drift speed) is low when B is large. Thus by applying a large bias field near Z = 0 the 50 percent limit on ohmic efficiency is reached when v is small i.e., when both the kinetic and ohmic energys are low. The B field is then decreased, at constant E, so that E/B increases thereby increasing the kinetic energy.

This behavior can be examined in more detail by assuming that the bias field varies inversely as the local pole face separation. A linearly divergent channel is used, as illustrated in Figure 2.

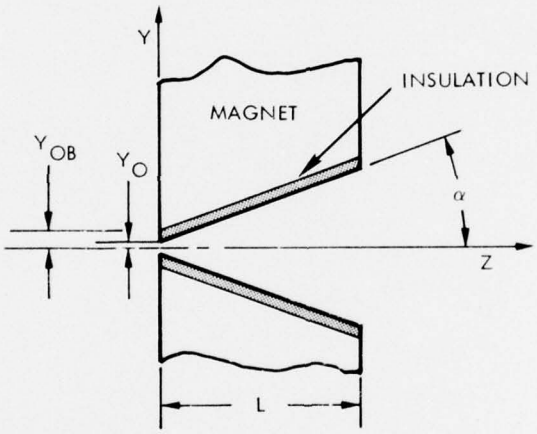

Figure 2. Accelerator Channel Geometry for Decreasing Bias Field

The distance from the centerline to the channel wall is y (at any Z) and the distance to the magnet pole face is y_B. If B_o represents the field strength at Z = 0, then the value at any Z is

$$B = B_o \frac{y_{oB}}{y_B}$$

but since

$$y_B = y_{oB} + Z \tan\alpha$$

it follows that

$$B = \frac{B_o}{1 + \frac{Z}{y_{oB}} \operatorname{Tan}\alpha} \tag{15}$$

Another consequence of the divergent channel geometry is that $\dot{m}$ is no longer constant. If $\dot{M}$ represents the total mass flow rate and h is the channel height then

$$\dot{M} = 2hy\dot{m}$$

since

$$y_Z = y_o\left(1 + \frac{Z}{y_o} \operatorname{Tan}\alpha\right)$$

$$\dot{m} = \frac{\dot{M}}{2hy_o\left(1 + \frac{Z}{y_o} \operatorname{Tan}\alpha\right)} \tag{16}$$

When Equations (15) and (16) are substituted into Equation (10), the acceleration relation becomes

$$\frac{dv}{dZ} = \frac{2hy_oB_o}{\dot{M}}\left(\frac{1 + \frac{Z}{y_o} \operatorname{Tan}\alpha}{1 + \frac{Z}{y_{oB}} \operatorname{Tan}\alpha}\right)j \tag{17}$$

Similarly the current density, from Equation (1), becomes

$$j = \sigma\left(E - \frac{vB_o}{1 + \frac{Z}{y_{oB}} \operatorname{Tan}\alpha}\right) \tag{18}$$

The circuit current is the integral of the current density over the electrode length L,

$$I = 2\int_0^L jydZ = 2y_o\int_0^L (1 + \frac{Z}{y_o}\,\mathrm{Tan}\,\alpha)jdZ \tag{19}$$

and the local plasma density is given by

$$\rho = \frac{\dot{M}}{2yhv} = \frac{\dot{M}}{2y_o hv\,(1 + \frac{Z}{y_o}\,\mathrm{Tan}\,\alpha)} \tag{20}$$

A numerical procedure can be used to calculate accerator efficiency by using Equation (18) to calculate j at an axial position Z where E, B_o and v are known. Equation (17) then gives dv/dZ and the velocity at an adjacent downstream station becomes

$$v + \Delta v = v + \frac{dv}{dZ}\Delta Z \tag{21}$$

2.2.1 Dimensionless Formulation

If the current density from Equation (1) is substituted into Equation (10), the acceleration relation becomes

$$\frac{dv}{dZ} = \frac{\sigma B}{\rho v}(E - vB)$$

or

$$\frac{dv}{dZ} = \frac{\sigma B^2}{\rho(\frac{v}{E/B})}(1 - \frac{v}{E/B}) \tag{22}$$

where E/B is the local drift speed. By making the initial value of B large (where the magnet gap is a minimum) the plasma speed approaches the drift speed in less than a millimeter. The remainder of the acceleration occurs with a small value for the difference term in Equation (22) multiplied by

a large coefficient. The magnitude of this coeffcient increases with the conductivity, with the square of the local bias field and with decreasing local density. This illustrates how a large bias field can compensate for a low conductivity.

This point can be seen in a different way by completing the dimensionless formulation of Equation (22). Thus

$$\frac{d\,\frac{v}{E/B}}{d\,\frac{Z}{L}} = \frac{\sigma L\, B^2}{\rho v}\left(1 - \frac{v}{E/B}\right) \tag{23}$$

where L is accelerator length, or since

$$\frac{\sigma L\, B^2}{\rho v} = \frac{\mu \sigma L v}{\left(\frac{v^2}{\frac{B^2}{\rho \mu}}\right)} = \frac{R_N}{M_A^2}$$

it follows that

$$\frac{d\,\frac{v}{E/B}}{d\,\frac{Z}{L}} = \frac{R_N}{M_A^2}\left(1 - \frac{v}{E/B}\right) \tag{24}$$

The Aflvén Mach number M_A is the ratio of the plasma velocity to the propagation speed of magnetic waves in the acceleration direction. By making this number small, through the use of a strong bias field, the effective Reynolds number is increased.

A more useful dimensionless formulation for calculation is to refer the velocity to the exit value of the drift speed rather than to the local value. Equation (23) then becomes

$$\frac{d\psi}{d\zeta} = \frac{2y_E hL\sigma B_E^2}{\dot{M}}\left(1 - \psi\frac{B}{B_E}\right)\left(\frac{B}{B_E}\,\frac{y}{y_E}\right) \tag{25}$$

where

$$\psi = \frac{v}{E/B_E}$$

$$\zeta = \frac{Z}{L}$$

$$\frac{B}{B_E} = \frac{1 + \frac{L}{y_{oB}} \operatorname{Tan}\alpha}{1 + \zeta \frac{L}{y_{oB}} \operatorname{Tan}\alpha}$$

$$\frac{y}{y_E} = \frac{1 + \zeta \frac{L}{y_o} \operatorname{Tan}\alpha}{1 + \frac{L}{y_o} \operatorname{Tan}\alpha}$$

and

$$\frac{2y_E h L \sigma B_E^2}{\dot{M}} = \left(\frac{R_N}{M_A^2}\right)_E$$

The values for R_N and M_A are found after a calculation is finished and ψ_E has been determined. Thus the exit values of R_N and M_A are given by

$$R_{NE} = u\sigma L\left(\psi_E \frac{E}{B_E}\right)$$

$$M_{AE}^2 = \frac{\left(\psi_E \frac{E}{B_E}\right)^2}{\left(\frac{B_E^2}{\rho_E \mu}\right)} = \frac{\left(\psi_E \frac{E}{B_E}\right)}{2y_E h\left(\frac{B_E^2}{\mu \dot{M}}\right)} \qquad (26)$$

From Equation (1) the dimensionless current density is

$$\frac{j}{\sigma E} = \left(1 - \psi \frac{B}{B_E}\right) \tag{27}$$

The circuit current is

$$I = \int 2yjdZ = 2y_o L\sigma E \int_0^1 \left(\frac{j}{\sigma E}\right) \left(1 + \zeta \frac{L}{y_o} \text{Tan}\alpha\right) d\zeta$$

or in dimensionless form

$$\frac{I}{2y_o L\sigma E} = \int_0^1 \frac{j}{\sigma E} \left(1 + \zeta \frac{L}{y_o} \text{Tan}\alpha\right) d\zeta \tag{28}$$

The input power is

$$W = IV = 2y_o hL\sigma E^2 \int_0^1 \left(\frac{j}{\sigma E}\right)\left(1 + \zeta \frac{L}{y_o} \text{Tan}\alpha\right) d\zeta$$

and the ohmic loss is

$$\Omega = \int \frac{2yh}{\sigma} j^2 dZ = 2y_o hL\sigma E^2 \int_0^1 \left(\frac{j}{\sigma E}\right)^2 \left(1 + \zeta \frac{L}{y_o} \text{Tan}\alpha\right) d\zeta$$

The ohmic efficiency is therefore

$$\eta = 1 - \frac{\Omega}{W} = 1 - \frac{\int_0^1 \left(\frac{j}{\sigma E}\right)^2 \left(1 + \zeta \frac{L}{y_o} \text{Tan}\alpha\right) d\zeta}{\int_0^1 \left(\frac{j}{\sigma E}\right)\left(1 + \zeta \frac{L}{y_o} \text{Tan}\alpha\right) d\zeta} \tag{29}$$

From Equation (29) a qualitative estimate of the efficiency is

$$\eta = 1 - \frac{j}{\sigma E} = \frac{v}{E/B}$$

or, from Equation (24)

$$\frac{d\eta}{d\zeta} = \frac{R_N}{M_A^2}(1 - \eta)$$

After integration this becomes

$$\eta = 1 - e^{-\frac{R_N}{M_A^2}} \tag{30}$$

A plot of this relation is shown in Figure 3. The efficiency is overestimated but the importance of the Reynolds number parameter is correctly illustrated.

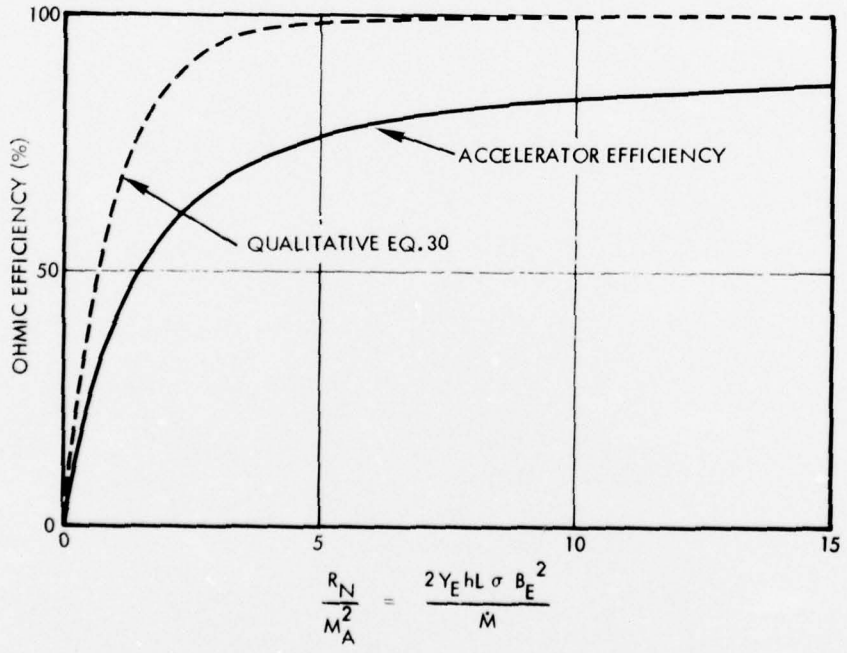

Figure 3. Effect of R_N/M_A^2 on Ohmic Efficiency
$(\frac{y_{oB}}{y_o} = 2, \frac{L}{y_o} = 10, \alpha = 20^o)$

2.2.2 Effect of Accelerator Parameters on Ohmic Efficiency

Figure 3 shows the effect of the parameter R_N/M_A^2 on ohmic efficiency for the geometric parameters $y_{oB}/y_o = 2$, $L/y_o = 10$ and $\alpha = 20^o$. At a value of 1.0 the efficiency is 40 percent, which agrees well with the self-field accelerator estimate. At a value of 10 the efficiency has increased to 84 percent. The corresponding accelerator parameters are plotted in Figure 4.

The effects on efficiency of the magnet to channel gap ratio, the channel length to gap ratio and the channel wall angle are shown in Figures 5 through 7, respectively. From Figure 5 it is seen that the gap ratio should be as small as possible for maximum efficiency. This means that the insulating walls separating the magnet pole faces from the plasma should be as thin as possible. Figure 6 shows that the channel length should be about 10 times the gap dimension.

The optimum length would require a tradeoff between efficiency and magnet weight, which increases with channel length.

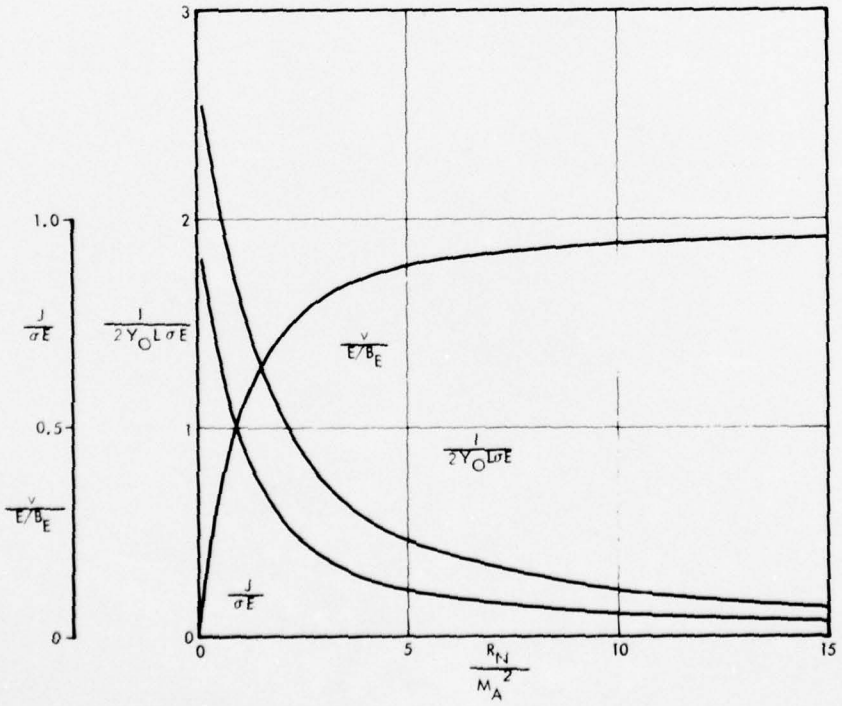

Figure 4. Dimensionless Accelerator Parameters vs $\frac{R_N}{M_A^2}$

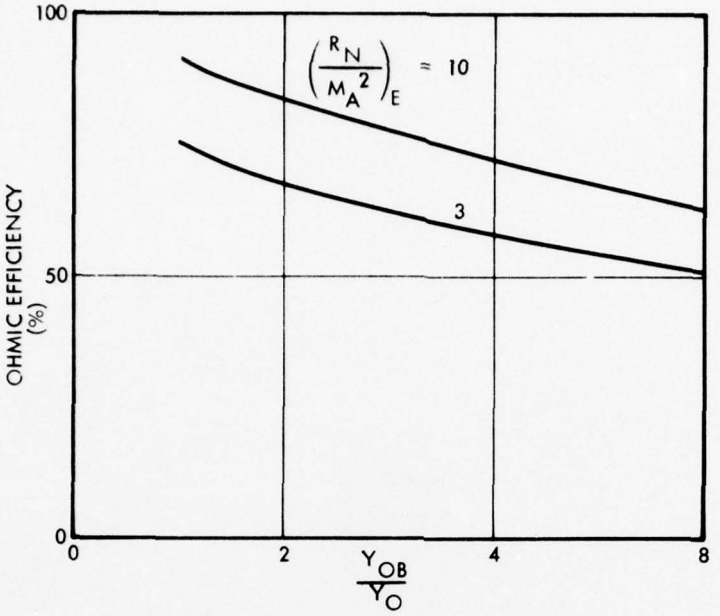

Figure 5. Effect of Magnet to Channel Gap Ratio on Efficiency at Two Values of $(R_N/M_A^2)_E$ ($\frac{L}{y_o}$ = 10, $\alpha = 20^o$)

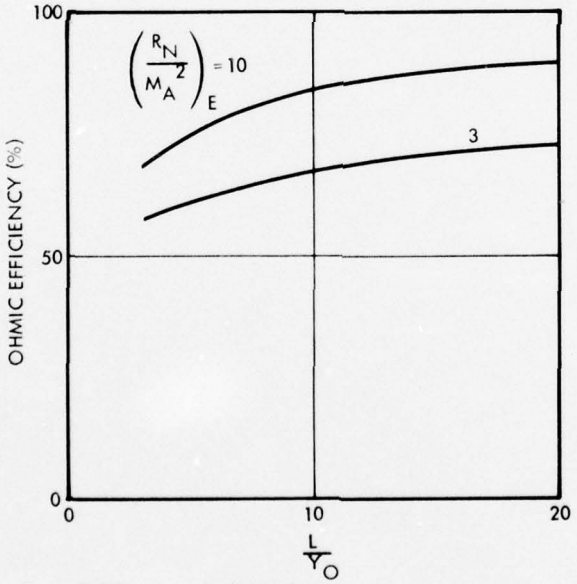

Figure 6. Effect of Accelerator Length on Efficiency at Two Values of $(R_N/M_A^2)_E$ ($y_{oB}/y_o = 2$, $\alpha = 20^o$)

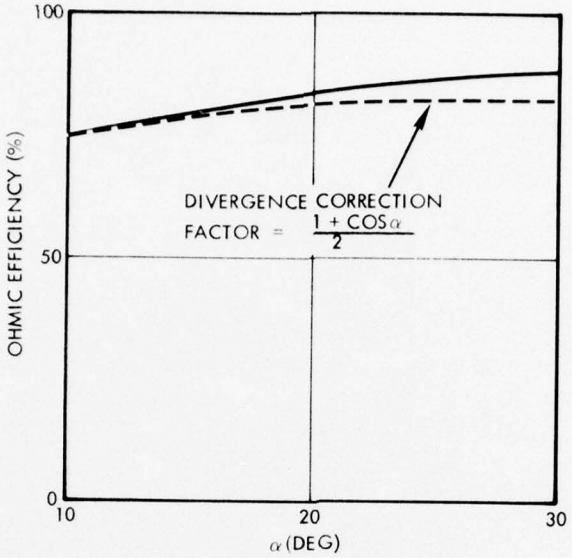

Figure 7. Effect of Channel Wall Angle on Efficiency ($\frac{Y_{oB}}{y_o} = 2, \frac{L}{y_o} = 10, \frac{R_N}{M_A 2} = 10$)

2.2.3 Effect of Dissociation and Ionization on Efficiency

The ohmic efficiency discussed in the previous section is an upper limit that does not consider the cost of dissociation and ionization. In a fully ionized plasma ohmic heat is dissipated by radiation while in a partially ionized gas it is the energy source that goes into dissociation and ionization. For any propellant there exists an I_{sp} high enough that the ohmic heating is greater than the energy needed for complete ionization. At an I_{sp} below that value the efficiency is governed by the cost of plasma formation. An upper limit can be found by requiring that the loss be equal to the energy of dissociation plus the energy required for first ionization. Thus if Φ represents this total cost, in electron volts,

$$\eta = \frac{1/2\ m_i (g\ I_{sp})^2}{1/2\ m_i (g\ I_{sp})^2 + e\Phi}$$

or

$$\eta = \frac{1}{1 + \frac{2e\Phi}{m_i\ (g\ I_{sp})^2}} = \frac{1}{1 + \frac{\beta}{I_{sp}^2}} \qquad (31)$$

where e is the electron charge and m_i is the ion mass.

Table 1 lists Φ for argon and three space storable propellants. In calculating Φ it was assumed that 15 ev is the first ionization cost for any ion, that O_2 dissociation costs 5 ev and that both H_2 and N_2 dissociation costs 10 ev.

Table 1. Cost of Plasma Production

Propellant	Φ (ev)	β (Sec^2)
Xenon	15	2.28×10^5
Argon	15	7.48×10^5
$N_2 O_3$	18.7	24.5×10^5
$N_2 + 2H_2$	20	74.9×10^5

Plots of efficiency versus I_{sp} are shown in Figure 8 for the propellant listed in Table 1 as calculated with Equation (31). The curves are terminated at 79 percent which is the ohmic efficiency calculated at $R_N/M_A^2 = 6$.

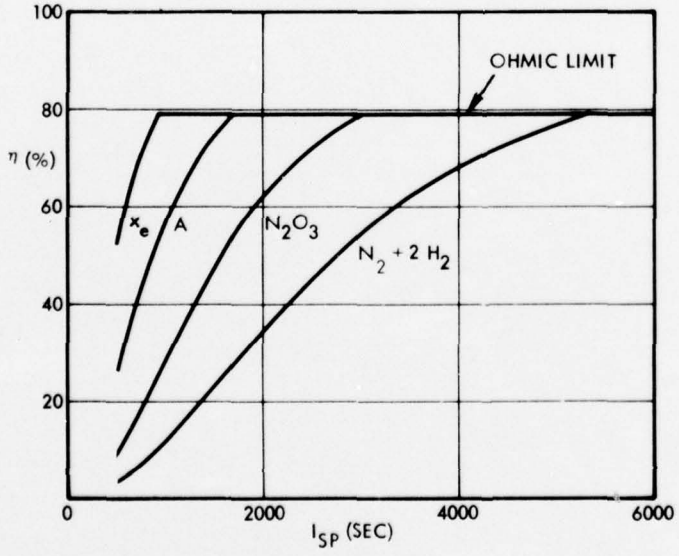

Figure 8. Calculated vs I_{sp} for $\frac{R_N}{M_A^2} = 6$

3. DESCRIPTION OF ACCELERATOR

Close-up views of the accelerator channel and permanent magnet are shown in Figures 9 and 10. The channel was mounted to a lucite plate leading to a 4 x 8 foot vacuum chamber as shown in Figure 11. Current for the discharge was supplied by the six element pulse line shown in Figure 12. The SCR used to switch the line can be seen in Figure 12. Each section of the line had 780 μF capacitance and 6 μH inductance. The total capacitance was 4680 μF and the pulse duration of the line was

$$\tau = 2\sqrt{LC} = 820\ \mu\ \text{sec}$$

3.1 ELECTRODE CHANNEL

The electrodes of the channel shown in Figure 9 were made of 1/4 inch thick brass and 1/16 inch thick glass plates were used for the side walls. Gas was admitted to the acceleration region through a sonic slit about 1/4 mm wide. The electrode separation was 2.5 cm. The electrode length in the flow direction was 3.2 cm for the first device tested. This was later shortened to 1.3 cm by covering the downstream portions with glass plates. The method of introducing the gas was altered during the testing. For the slit injection geometry a sealed plenum box was fitted over the accelerator and pressurized with argon. In later tests the sonic slit was closed and 2.5 mm diameter holes were drilled near the apex of the upper and lower electrodes. These holes were connected to high pressure lines that led directly to the pressure regulated gas supply.

3.2 MAGNET

Recently developed Brown-Bovari samarium-cobalt permanent magnets were used to drive the bias field magnetic circuit. A demagnetization curve for this material is shown in Figure 13. As shown in Figure 10, eight magnet blocks were used in the structure (four in parallel and two in series). The configuration shown has large leakage flux and could be made lighter for a practical thruster.

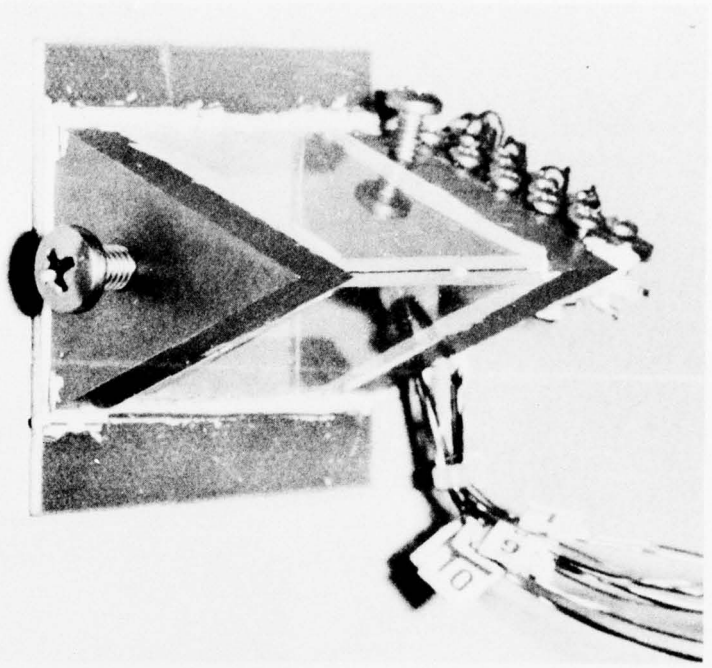

Figure 9. Acceleration Channel

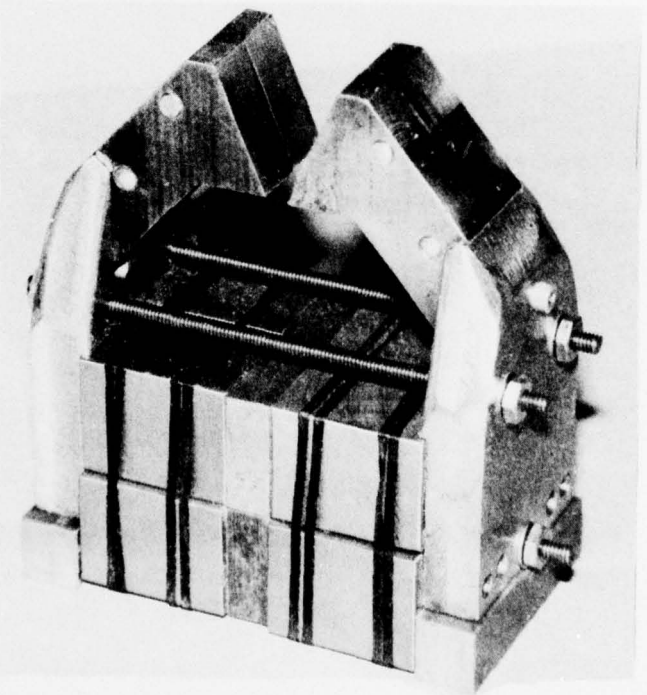

Figure 10. Bias Field Magnet

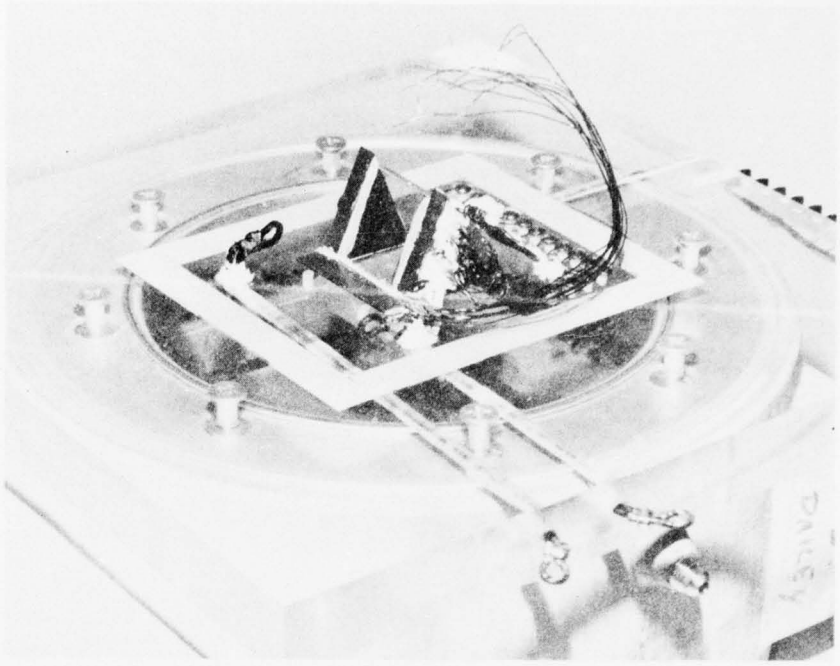

Figure 11. Accelerator Channel Mounted on Vacuum Chamber

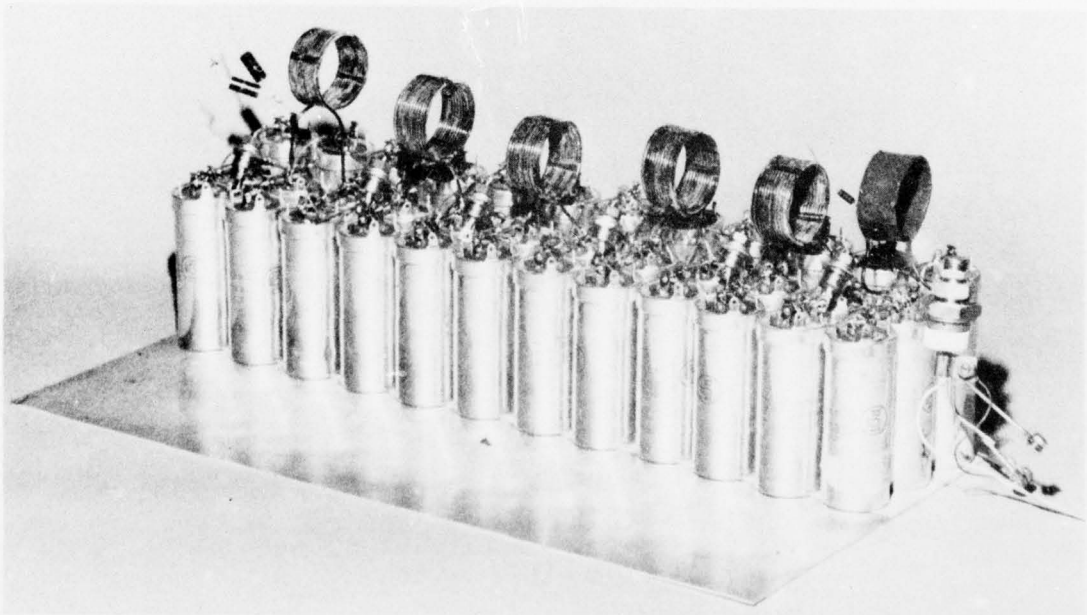

Figure 12. Six-Section Pulse Line

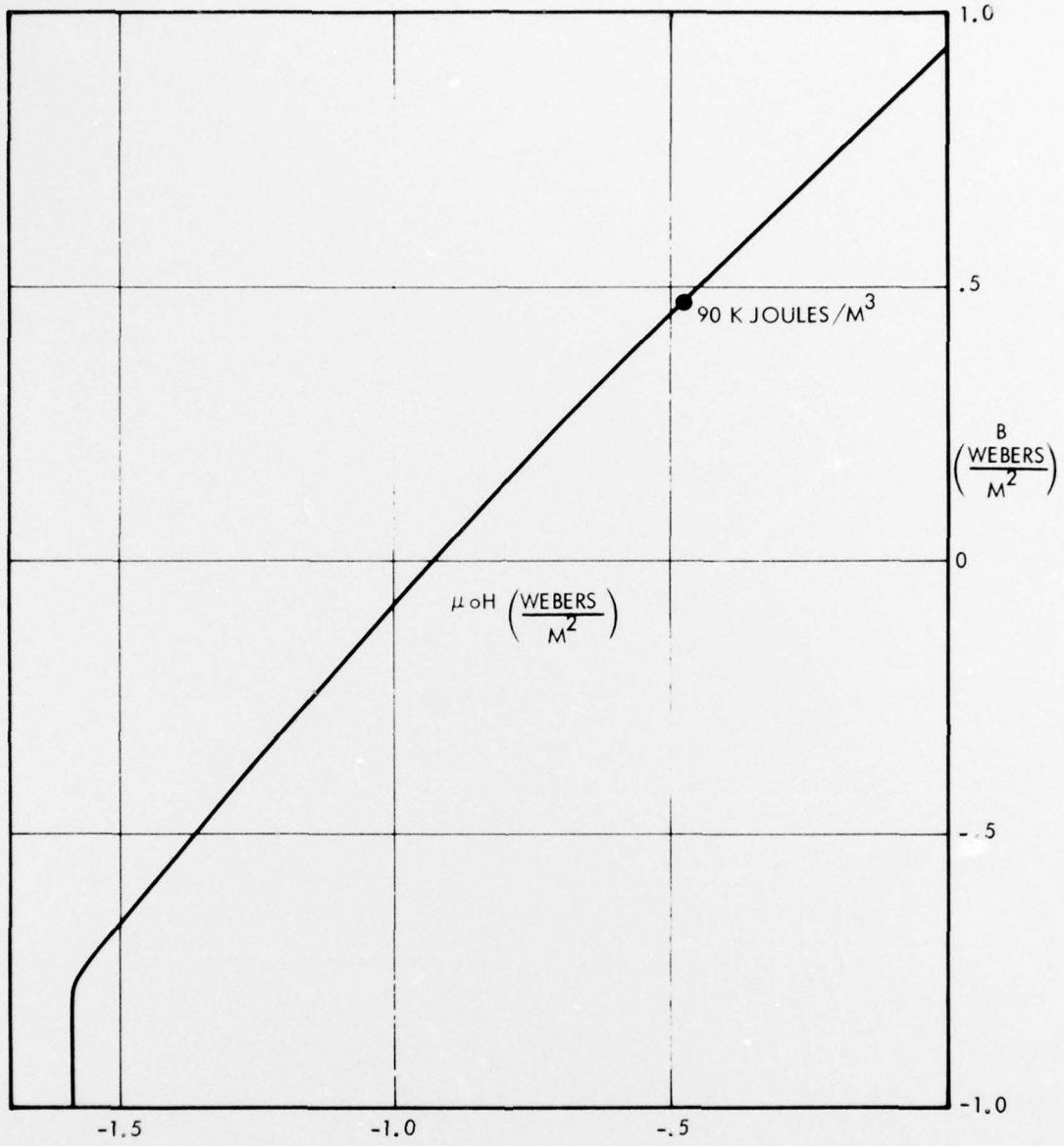

Figure 13. Demagnetization Curve for Brown-Bovari Samarium Cobalt Magnets

The original design used four magnet blocks with a minimum gap spacing of 0.19 cm. The field measurements plotted in Figure 14 show that high fields were obtained for the first few millimeters with low values near the exit. The gap was opened to 0.51 cm to provide enough room for the

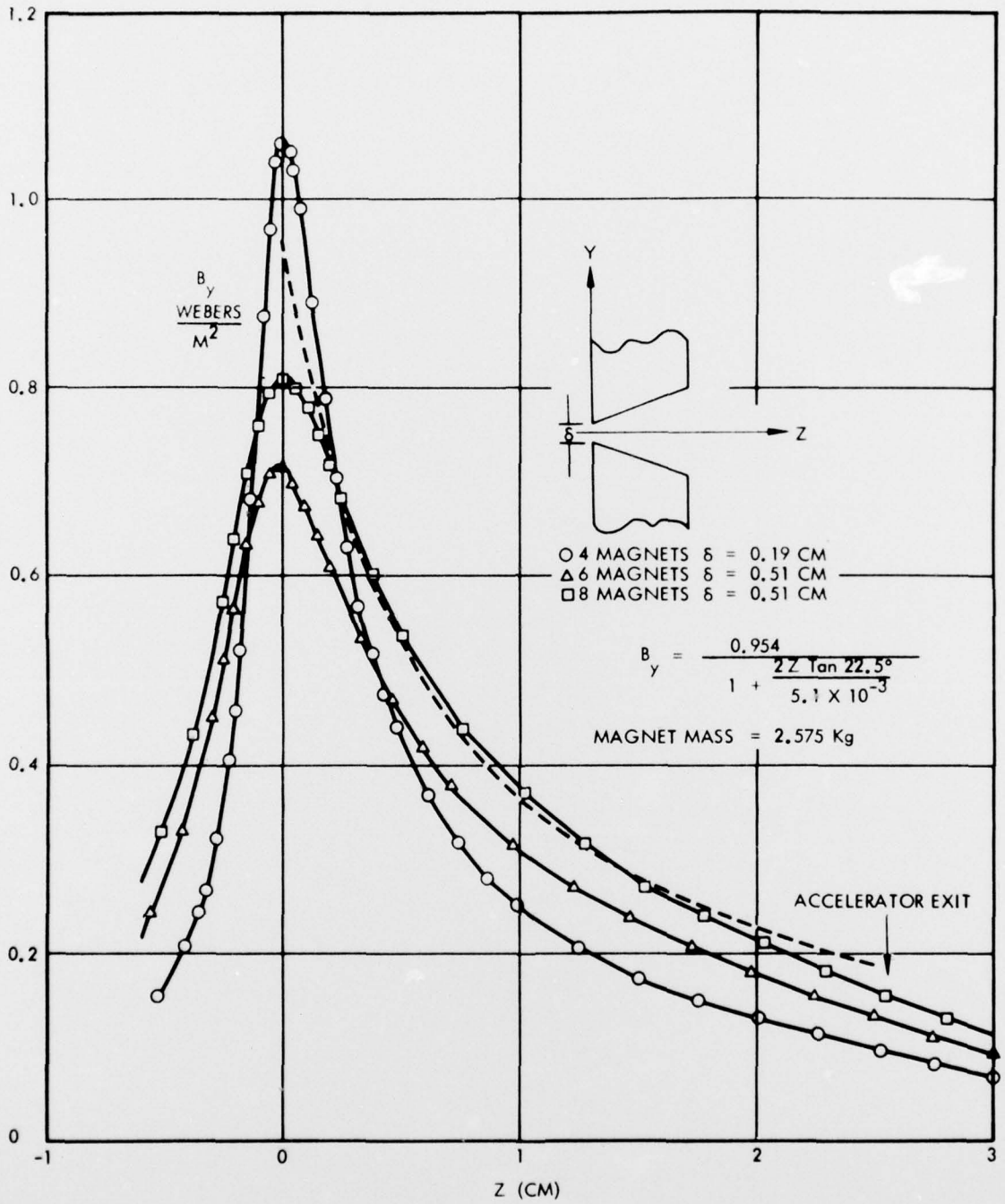

Figure 14. Magnetic Field at ℄ for Different Magnet Configuration

glass side walls so that the apex of the plasma volume would be near the leading edge of the pole pieces. Field strength plots are shown in Figure 14 for four, six, and eight magnet blocks. The latter configuration was used for the experiments. As shown in the figure, the field along the axis is prescribed reasonably well by the relation

$$B_y = \frac{0.954}{1 + \frac{2z \text{ Tan } 22.5^0}{0.51}} \tag{32}$$

The lateral variation of the magnetic field across the gap was measured at several positions to determine the uniformity of the field at a given axial station. The results, plotted in Figure 15, show that the variation is reasonably small.

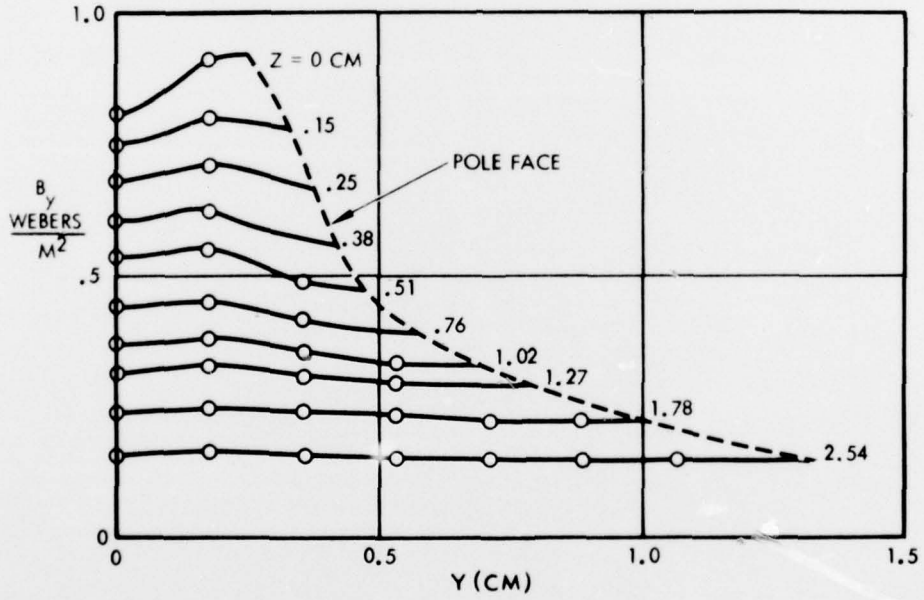

Figure 15. Variation of Magnetic Field Across Magnet Gap for Several Axial Stations (Eight Magnets, $\delta = 0.51$ cm)

4. EXPERIMENTAL RESULTS

Measured efficiencies are shown as a function of I_{sp} in Figure 16. The theoretical curve from Figure 8, based on the optimistic assumption of a first ionization loss only, is shown for comparison. Also shown in Figure 16 are efficiencies for a self-field pulsed Teflon thruster[1] and a 30 cm ion engine[2].

The measured efficiency for the bias field thruster is only slightly less than the theoretical estimate and is considerably greater than that of the self-field plasma thruster and the ion engine.

4.1 IMPULSE MEASUREMENT

The experimental efficiency was found from the relation

$$\eta = \frac{Mv^2}{2J} = \frac{MVgI_{sp}}{2J}$$

or

$$\eta = \frac{\Delta I g I_{sp}}{2J} \tag{32}$$

where ΔI is the impulse per shot, M is propellant ejected per shot and J is the product of voltage and current at the electrode terminals integrated over the discharge period. The I_{sp} was found from the relation

$$I_{sp} = \frac{\Delta I}{Mg} \tag{33}$$

The mass flow rate into the thruster was calculated using the measured fill-up rate of the vacuum chamber at constant supply pressure.

The impulse bit ΔI was determined by suspending the magnet structure from a pair of 1.4 meter long piano wires and measuring its deflection when the thruster was fired. The deflection was of the order of 2 mm and could be read with a repeatibility of ± 5 percent.

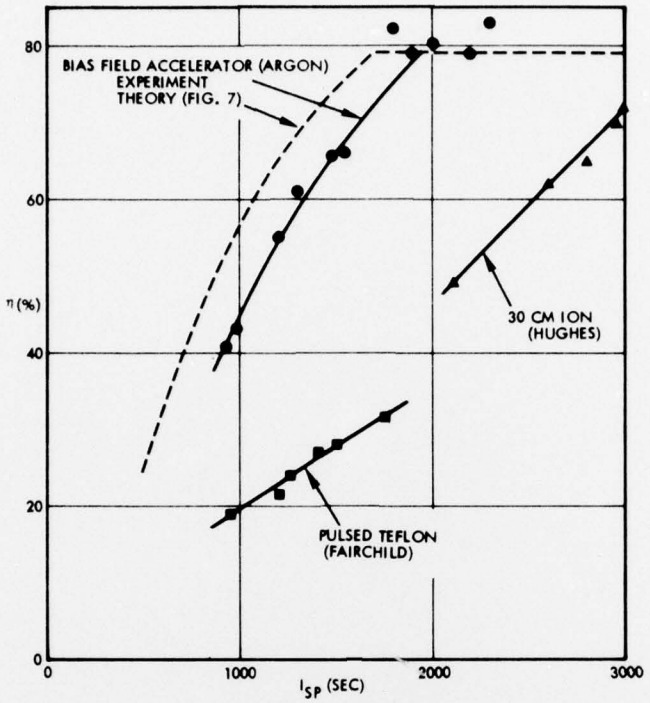

Figure 16. Comparison of Measured Efficiency with Theory and with Other Thrusters

An independent measurement of impulse was made by collecting the accelerated plasma in a 12 inch diameter by 16 inch long cylinder of aluminum foil suspended from threads inside the vacuum chamber. Four threads were used, attached to a lightweight frame to which the cylinder was mounted. This method of suspension minimized the oscillations that were induced by the high velocity gas flow through the accelerator before the capacitor bank was discharged. The data reading technique was first to observe the position of a pointer attached to the cylinder relative to a meter stick in the vacuum chamber with no gas flow, then to estimate the maximum deflection in the gas stream before and after the discharge. From the known geometry of the suspension the increase in potential energy was calculated.

The results of this measurement are shown in Figure 17. In spite of the large data scatter due to the unsteadiness of the cylinder in the gas stream, it can be seen that momentum loss due to electrode drag is not a big effect. For the present feasibility study it is ignored and thrust measurements are based on the magnet impulse balance data.

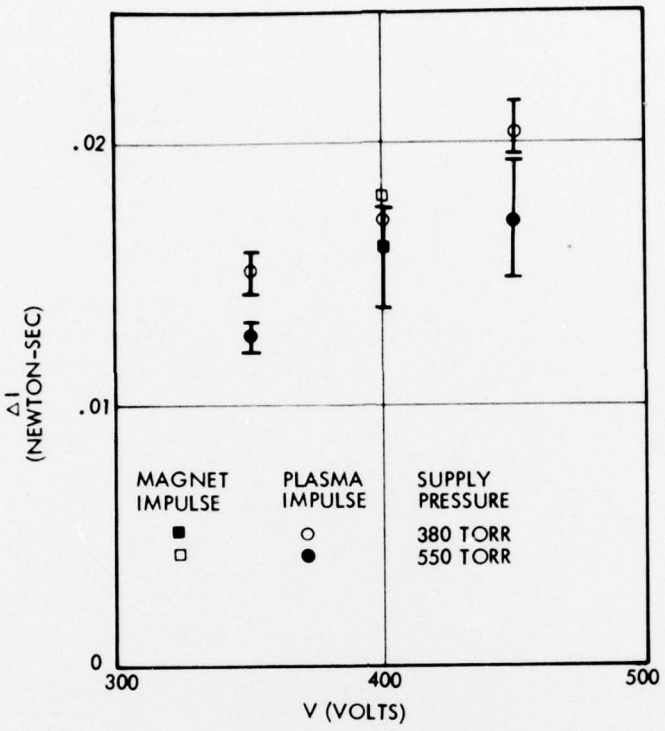

Figure 17. Comparison of Magnet Impulse and Plasma Impulse Measurements

4.2 CIRCUIT MEASUREMENTS

The input energy in the denominator of Equation (33) was measured by integrating the product of the circuit current and the voltage across the electrodes for each test condition. A typical oscillograph record is shown in Figure 18. A pair of voltage probes and a differential amplifier were used for the voltage data while the voltage drops across a low impedance series resistor (0.167 mΩ) was used to measure current. The accelerator impedance for this case is seen to be about 50 mΩ.

4.3 DIAGNOSTIC MEASUREMENTS

As can be seen from Equation (32) the ratio of η to I_{sp} is independent of the mass accelerated and depends only on measurements of ΔI and J. Measurements with the first accelerator tested gave I_{sp} values calculated from Equation (33) that led to efficiencies from Equation (32) well over 100 percent. There were two possible explanations. One was that the current ran partly along the glass sidewall and the other was that additional mass

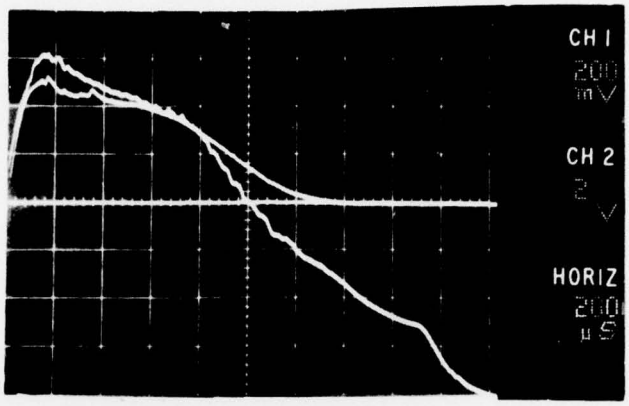

Figure 18. Current (Upper Trace) and Terminal Voltage (Lower Trace) for a Typical Discharge (20 V/cm, 1200 A/cm)

was added by ablation. The plasma impulse measurement eliminated the first of these possibilities. To examine the second one, a small magnetic field probe was built and used to measure the axial field within the accelerator. Figure 19 shows lateral distribution at three axial positions. The peaking of the field within the plasma also shows that the current is within the plasma and not on the sidewalls. However the field strength should have decreased steadily in the downstream direction instead of showing a large value at the 2.9 cm station. An axial distribution was then run with the probe at the sidewall. The result, shown in Figure 20, has a strong peak at 2.5 cm. This is near the downstream edge of the electrode where an epoxy – fiberglass plate was used in assembling the thruster. Inspection showed extensive charring of the plate had occurred. Evidently mass addition by ablation of the plate contributed to the incorrect measurement of efficiency and I_{sp}.

Four glass plates were attached to the inner surfaces of the accelerator that covered the plate and electrodes except for the first 1.3 cm downstream from the apex. This modification isolated the epoxy fiberglass plate from the discharge and prevented further ablation. However efficiencies greater than 100 percent were again observed indicating that spurious mass addition must still be occurring.

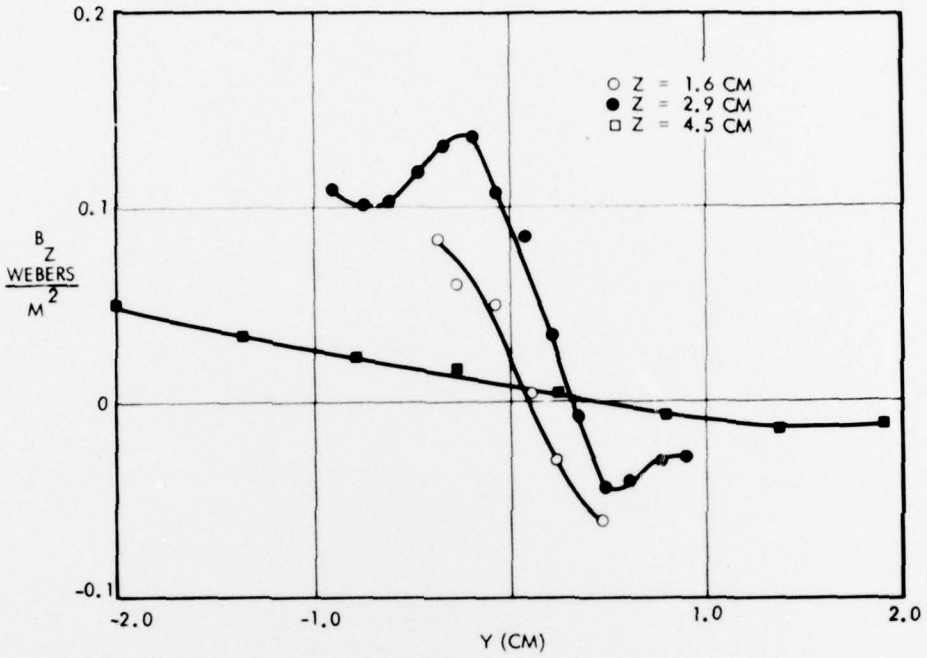

Figure 19. Lateral Variation of Axial Magnetic Field (No Glass Covers)

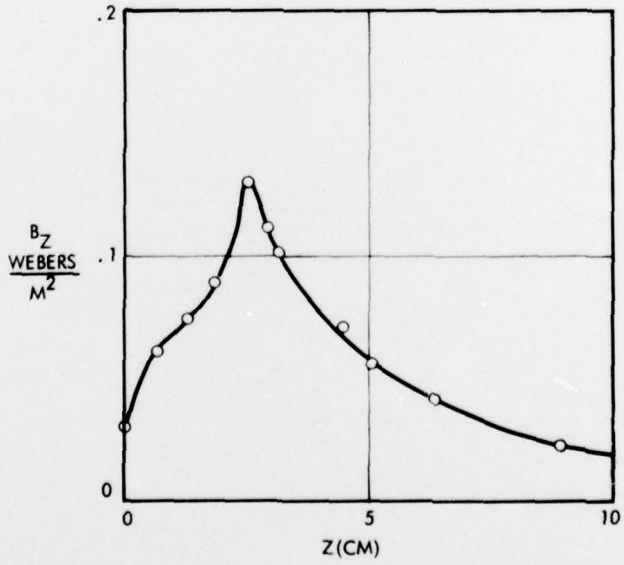

Figure 20. Axial Variation of Axial Magnetic Field at Side Wall

A miniature Rogowsky probe was built to permit the direct measurement of plasma current. It was roughly rectangular in shape with 5 cm long sides spaced 0.5 cm apart; the long dimension was in the axial direction. An axial scan of the total current passing through the probe window is plotted in Figure 21. It can be seen that no current was running forward of the 1 cm position, i.e., the measured current remained constant to that axial station. It then decreased rapidly, falling to 20 percent at 2 cm. Apparently the plasma current was concentrated in a layer a few mm wide at about 1 cm from the apex. It was suspected that epoxy, that was used to seal the slit at the apex (between the glass side plates) was supplying mass by ablation. Current was prevented from running in the first 1 cm by the high mass density there.

This region was covered by placing another glass plate against the inside surface of one of the sides and moving it forward to close off the slit. A plasma current scan was then made and the results plotted in Figure 21 for comparison with the uncovered slit. The data extrapolate to about 1000 amperes at Z = 0. The measured circuit current for this test

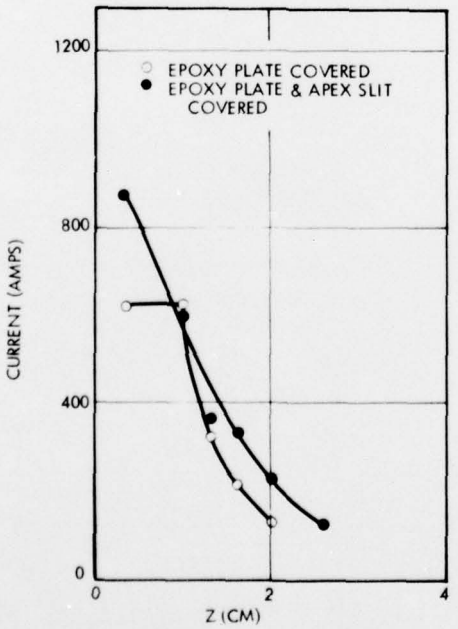

Figure 21. Axial Variation of Current in Rogowsky Probe (450 volts)

was 3200 amperes. Since the probe area covered about one third of the current-carrying cross-section, the probe measurement indicates that the current density was roughly constant for the clean configuration having all of the epoxy surfaces covered. The efficiency versus I_{sp} data shown in Figure 16 were measured for this configuration.

5. CONCLUSIONS

1. High acceleration efficiencies have been shown to be feasible for the bias field accelerator. A value of 80 percent at 2000 seconds I_{sp} has been measured.

2. High efficiency can only be achieved by using a bias field that decreases in the direction of acceleration. The ohmic efficiency is limited to 50 percent for a constant bias field, as it is for a self-field accelerator having no bias field.

3. By comparing the measured plasma momentum to the impulse delivered to the bias field magnet, it was found that electrode drag has a relatively small effect; no consistent effect greater than the experimental error was observed.

4. The accelerator operated well with sonic circular orifices in the electrodes, near the apex. Further measurements should be made with gas fed through a sonic slit at the apex and between the electrodes.

5. Detailed probe measurements throughout the plasma volume are needed to better understand the acceleration processes. Also additional work is needed to increase the accelerator impedance so that it can operate with light weight film capacitors.

REFERENCES

1. D. Palumbo, Personal Communication.

2. H.J. King, et al, "Low Voltage 30-cm Ion Thruster Development," NASA CR-134731. October 1974.

SECURITY CLASSIFICATION OF THIS PAGE (When Data Entered)

REPORT DOCUMENTATION PAGE

READ INSTRUCTIONS BEFORE COMPLETING FORM

1. REPORT NUMBER: AFOSR-TR-77-0828	2. GOVT ACCESSION NO.
3. RECIPIENT'S CATALOG NUMBER	
4. TITLE (and Subtitle): PULSED PLASMA LOSS AND ACCELERATION MECHANISMS IN STRONG BIAS MAGNETIC FIELDS	5. TYPE OF REPORT & PERIOD COVERED: INTERIM rept. 1 June 1976–31 May 1977
	6. PERFORMING ORG. REPORT NUMBER
7. AUTHOR(s): C. L. DAILEY, R. H. LOVBERG	8. CONTRACT OR GRANT NUMBER(s): F44620-76-C-0107
9. PERFORMING ORGANIZATION NAME AND ADDRESS: TRW DEFENSE AND SPACE SYSTEMS GROUP, ONE SPACE PARK, REDONDO BEACH, CALIF. 90278	10. PROGRAM ELEMENT, PROJECT, TASK AREA & WORK UNIT NUMBERS: 2308A1, 61102F
11. CONTROLLING OFFICE NAME AND ADDRESS: AIR FORCE OFFICE OF SCIENTIFIC RESEARCH/NA, BUILDING 410, BOLLING AIR FORCE BASE, D.C. 20332	12. REPORT DATE: JULY 1977; 13. NUMBER OF PAGES: 36
14. MONITORING AGENCY NAME & ADDRESS (if different from Controlling Office): 39 p.	15. SECURITY CLASS. (of this report): UNCLASSIFIED; 15a. DECLASSIFICATION/DOWNGRADING SCHEDULE

16. DISTRIBUTION STATEMENT (of this Report)

Approved for public release; distribution unlimited

17. DISTRIBUTION STATEMENT (of the abstract entered in Block 20, if different from Report)

18. SUPPLEMENTARY NOTES

19. KEY WORDS (Continue on reverse side if necessary and identify by block number)

PLASMA GENERATOR
PLASMA ACCELERATOR
PULSED PLASMA THRUSTER
JXB PLASMA ACCELERATOR
ELECTRIC PROPULSION
SPACE PROPULSION
SATELLITE POSITIONING AND MANEUVERING

20. ABSTRACT (Continue on reverse side if necessary and identify by block number)

RESULTS OF THE FIRST YEAR OF A STUDY OF PLASMA ACCELERATION IN THE PRESENCE OF A STRONG APPLIED BIAS MAGNETIC FIELD ARE DESCRIBED. A THEORETICAL MODEL HAS SHOWN THAT ACCELERATION EFFICIENCY IS LIMITED TO 50% FOR A CONSTANT FIELD STRENGTH. HOWEVER, IT CAN BE INCREASED TO MORE THAN 80% BY APPLYING A BIAS FIELD THAT DECREASES IN THE DIRECTION OF ACCELERATION. EXPERIMENTS WITH ARGON IN AN ACCELERATOR OF THIS TYPE ARE DESCRIBED WHICH SHOW AN ACCELERATION EFFICIENCY INCREASING WITH Isp TO A VALUE OF 80% AT 2000 SECONDS Isp. STEADY GAS →

DD FORM 1 JAN 73 1473 EDITION OF 1 NOV 65 IS OBSOLETE

409637

UNCLASSIFIED
SECURITY CLASSIFICATION OF THIS PAGE (When Data Entered)

FLOW WAS USED FOR THE EXPERIMENTS WITH CURRENT SUPPLIED FOR 0.8 M SEC FROM A PULSE LINE. IMPULSE WAS INDICATED BY THE DEFLECTION OF THE BIAS FIELD MAGNET WHICH WAS SUSPENDED AS AN IMPULSE PENDULUM.